Experimental investigation of torque measurement in hermetic compressor

IOP Conf. Series: Materials Science and Engineering **604** (2019) 012056 doi:10.1088/1757-899X/604/1/012056

Experimental investigation of torque measurement in hermetic compressor

J Xu[1,2], P Liu[2], L P Ren[1,2], L C Kong[2]

[1]State Key Laboratory of Air-conditioning Equipment and System Energy Conservation, ZhuHai, Guangdong 519070, China
E-mail: luip363216@126.com
[2]Gree Electric Appliances, Inc.
ZhuHai, Guangdong 519070, China

Abstract. In order to measure the compressor torque accurately and guide the design efficiently, a torque measurement method for the hermetic compressor is proposed. Then the shaft power measuring system is established by using a virtual instrument developed by LabVIEW. The stability of slip ring is monitored in real time through an external static full bridge circuit for eliminating the influence of its unstable contact resistance on measurement during the working process. The experimental results indicate that the change of contact resistance cannot be neglected in measuring process. The experimental torque curve is in agreement with the theoretical one. The measured shaft power of the prototype is 320W, finally the motor efficiency and the mechanical efficiency is 91.7% and 89.1%, respectively.

1. Introduction

As the basic load form of the drive shaft, torque is an important parameter in design process of the compressor motor, and it directly reflects performance of the compressor. Therefore, it is of great significance and practical value to measure the shaft torque during compressor operation [1].

Based on measurement principle, the torque measuring method can be divided into three categories: phase difference, magneto-elastic and strain [2-3]. The strain method has the advantages of simple structure, low cost, mature technology, etc. It has been widely used, and become a mainstream torque measuring method in current engineering field. There are two types of the strain method, in which the non-contact type uses wireless telemetry technology to realize data acquisition through wireless transceiver chip [4-5]. This method is simple in assembly, stable in operation and long in service life, which has been widely used for dynamic torque measurement of mechanical power transmission systems. However, the internal space of a hermetic compressor is limited. So the application of non-contact method requires a large change in original structure of the compressor. The measuring environment is harsh (high temperature and pressure, corrosive refrigerant, electromagnetic interference, lubricating oil, etc.), which makes it impossible to establish a wireless telemetry system inside the compressor.

M. Matsushima et al. [6] studied shaft torque measurement of compressor and obtained the torque curve in each running period. Therefore, in this paper the torque measuring system is designed by contact strain measuring method, and transmits strain signal out of compressor through the slip ring to achieve data acquisition. However, the slip ring will have a great influence on torque measurement due to its

unstable contact resistance during operating process [7-8], and there are few studies in this area.

In order to eliminate the influence of slip ring on measurement, an eight-channel slip ring is used to monitor its stability while measuring shaft torque through a static full bridge circuit outside the compressor. Finally, through data processing, a stable torque signal can be obtained. Then power distribution of the compressor is analyzed in combination with the measured torque result.

2. Testing Principle

The torque measurement uses full bridge circuit. So divide four foil strain gauges into two groups, and then they will be 180˚ symmetrically pasted on surface of the shaft. Wherein, each strain gauge has a 45˚ angle between the axial line and itself, as shown in Figure 1.

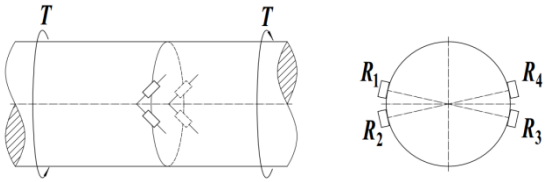

Figure 1 Diagram of strain gauge patch

According to material mechanics, there will be

$$T = \frac{\pi E \varepsilon_{\max} D^3 (1-\alpha^4)}{16(1+\mu)} \tag{1}$$

Wherein： T —— torque;
E —— young's modulus;
D —— diameter of the shaft;
α —— ratio of inner and outer diameter;
μ —— poisson ratio.

An eight-channel slip ring is used to transmit signals of the rotating crankshaft, and the schematic diagram of the structure is shown in Figure 2. Contact resistance is one of the most important parameters of the slip ring, which directly affects its performance. During the operation of the compressor, the variation in the deflection of the crankshaft leads to the change of the contact pressure between the slip ring brush and the metal ring, thereby causing a dynamic response in contact resistance. In addition, with the increasing of the running time, the rising temperature of the slip ring brush increases the contact resistance. In order to overcome the influence on torque measurement caused by unstable contact resistance of the slip ring during operating process, a static unstressed full bridge circuit is placed outside the compressor, which is the slip ring calibration bridge circuit. By connecting this bridge circuit to the slip ring, its stability of contact resistance can be monitored synchronously while the shaft torque is being measured. This method of measuring bridge circuit is shown in Figure 3.

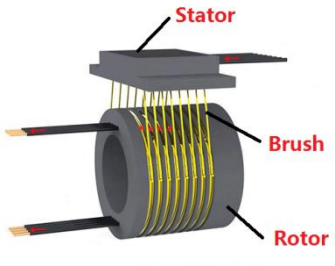

Figure 2 Schematic diagram of the slip ring

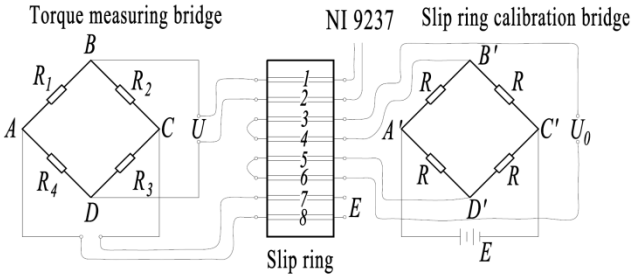

Figure 3 Diagram of measuring bridge circuit

The slip ring calibration bridge circuit is composed of four identical strain gauges and is attached to

an unstressed specimen surface. From the previous test experience, it is found that input end of the bridge circuit is not affected by slip ring, so only two output ends of the calibration bridge circuit are connected to slip ring. Specifically, after B' point is taken out through channel 4, channel 3 short-circuit with 4, and then connect to the measuring equipment after channel 3 is taken out, and D' point is in the same way.

Since the torque measuring bridge circuit is inside the compressor, the input end and output end of this bridge circuit must pass through slip ring. So measuring equipment is connected with A, B, C and D in the bridge circuit using the remaining 4 channels.

3. Theoretical Torque Calculation

In order to guide the actual measurement of shaft power and to judge accuracy of the measurement data, it is necessary to calculate theoretical torque T_{th} of compressor. That is, the ideal torque with 100% volumetric efficiency and 100% adiabatic efficiency. It is generally believed that theoretical torque mainly includes the torque generated by compression of gaseous refrigerant T_g. But there is a pressure gradient force caused by different gas pressure on two sides of the vane which will generate negative torque T_v. So, T_{th} will be

$$T_{th} = T_g + T_v \tag{2}$$

According to the geometric relationship in Figure 4, there is

$$T_g = F_g l \tag{3}$$

The gas force acting on arcs AA' and TT' mutually counteracts each other. Gas force acting on arc AT is the compressor chamber pressure P_θ, and gas force acting on arc $A'T'$ is the suction chamber pressure P_{s0}. The resultant force F_g points to suction chamber, namely

$$F_g = RL(1-\tau)(P_\theta - P_{s0})\left[2(1-\cos\theta) + \frac{\tau}{1-\tau}(1-\cos 2\theta)\right]^{1/2} \tag{4}$$

Wherein： R —— cylinder radius;
L ——axial length of roller;
τ —— deflection ratio.

The relationship between volume and pressure satisfies the process equation, and polytropic index of compression process is n, so

$$P_\theta = P_{s_0}\left(\frac{V_\beta}{V_\theta}\right)^n \tag{5}$$

Wherein： V_θ —— element volume at rotation angle θ;
V_β—— element volume at start of compression;
P_θ—— gas pressure in element volume at rotation angle θ;
P_{s0}—— suction pressure.

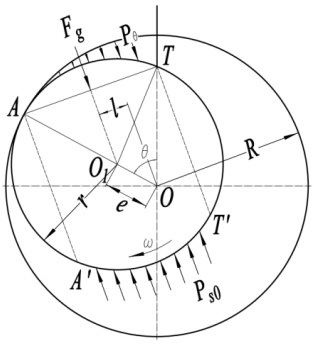

Figure 4 Force analysis of roller

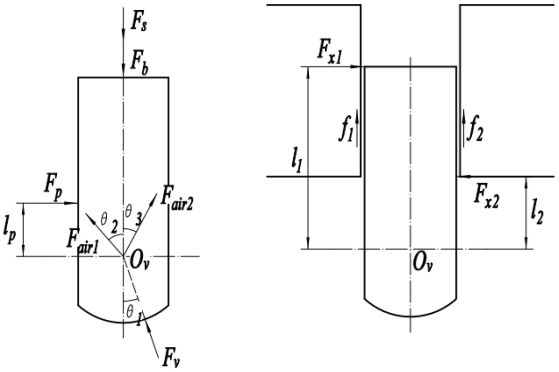

Figure 5 Force analysis of vane

Figure 5 shows the force acting on vane, so F_{x1} and F_{x2} can be obtained by the equilibrium equation, namely

$(0 \sim \pi)$：

$$F_{x1} = \frac{\left(\frac{\mu B}{2} + l_2\right)F_{x2} - F_p l_p}{\frac{\mu B}{2} + l_1}$$

$$F_{x2} = \frac{(F_x \cos\theta_1 - F_y \sin\theta_1)\left(\frac{\mu B}{2} + l_1\right) - (\cos\theta_1 + \mu \sin\theta_1)F_p l_p}{(\cos\theta_1 - \mu \sin\theta_1)\left(\frac{\mu B}{2} + l_1\right) - (\cos\theta_1 + \mu \sin\theta_1)\left(\frac{\mu B}{2} + l_2\right)} \tag{6}$$

$(\pi \sim 2\pi)$：

$$F_{x1} = \frac{\left(\frac{\mu B}{2} - l_2\right)F_{x2} + F_p l_p}{\frac{\mu B}{2} - l_1}$$

$$F_{x2} = \frac{(F_x \cos\theta_1 - F_y \sin\theta_1)\left(\frac{\mu B}{2} - l_1\right) + (\cos\theta_1 - \mu \sin\theta_1)F_p l_p}{(\cos\theta_1 + \mu \sin\theta_1)\left(\frac{\mu B}{2} - l_1\right) - (\cos\theta_1 - \mu \sin\theta_1)\left(\frac{\mu B}{2} - l_2\right)} \tag{7}$$

Wherein：μ —— friction coefficient;
B —— width of vane;
l_1 —— force arm between F_{x1} and circle center of vane tip;
l_2 —— force arm between F_{x2} and circle center of vane tip;
l_p —— force arm between F_p and circle center of vane tip;
θ_1 —— angle between F_v and y axis;
F_{x1}, F_{x2} —— supporting forces acting on vane;
F_p —— pressure gradient force acting on vane;
F_x, F_y —— resultant forces along x axis and y axis;

Based on Figure 5, the force between vane and roller F_v can be obtained.

$$F_v = \frac{(\mu F_x + F_y - 2\mu F_{x_2})}{(\cos\theta_1 + \mu \sin\theta_1)} = \frac{(\mu F_x + F_y + 2\mu F_{x_1})}{(\cos\theta_1 + \mu \sin\theta_1)} \tag{8}$$

From the geometric relation in Figure 4, there will be

$$l_v = \left[e\cos\theta + (r + R_h)\cos\theta_1\right]\sin\theta_1 \tag{9}$$

So, the negative torque generated by vane is

$$T_{\mathrm{v}} = F_{\mathrm{v}} l_{\mathrm{v}} \tag{10}$$

According to the above derivation, theoretical torque curve is shown in Figure 6.

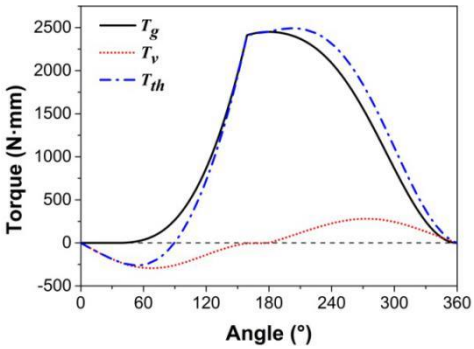

Figure 6 Theoretical torque curve

As can be seen from Figure 6, the pressure in compression chamber is low within the rotation angle of 0~90˚. At this time, the torque T_{v} generated by acting force between vane and shaft force is dominant, resulting in a negative shaft torque T_{th}.

A simple theoretical model is proposed to evaluate the change in crankshaft torque during compressor operation. In fact, due to the complex working condition, it is hard to consider the effect of many influencing factors theoretically, such as leakage, mechanical loss, exhaust loss, etc., while those effects are analyzed by experiments below.

4. Experiment

4.1. Prototype

The prototype is shown in Figure 7. The displacement of the test prototype is 9.1 cc. The type of anti-magnetic strain gauge is ZEMIC TBM120-3HA, with a resistance of 120Ω and a sensitivity factor of 2.11. It has good temperature self-compensation and anti-electromagnetic interference performance. Araldite® AV 138 M epoxy resin is used as a protective coating to prevent adverse effects of the refrigerant and lubricant inside the compressor. The high performance strain gauge adhesive H-610 is used to protect the testing from interference due to temperature variations. H-610 has the characteristics of small creep, low hysteresis, good repeatability and wide operating temperature range. According to the strict solidification time of H-610, it can ensure that the strain gauges work stably in the temperature range of -226~200˚C. The measurement signal is acquired by NI cDAQ-9184 and NI 9237 acquisition systems at a sampling frequency of 50000 Hz. The slip ring is customized, with eight channels, shielded design and certain anti-interference ability. Its shell is made of aluminum alloy and has good corrosion resistance, with protection grade IP65, good sealing and working temperature -40~200℃, the maximum speed is 5400rpm.

The voltage signal generated by torque measurement bridge circuit is transmitted out of the compressor through a slip ring which is installed on the top of the compressor. Then it is converted into a digital signal by a data acquisition card with a built-in amplifier, and finally displayed and stored in computer terminal. Since the torque measuring point is located between motor and pump body, in order to enable the wire of slip ring to reach that point, the shaft needs to be processed into a hollow structure.

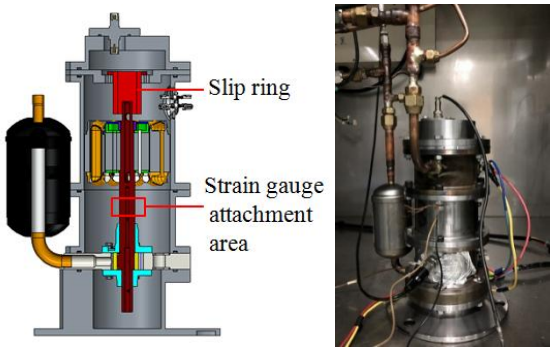

Figure 7 Diagram of the prototype

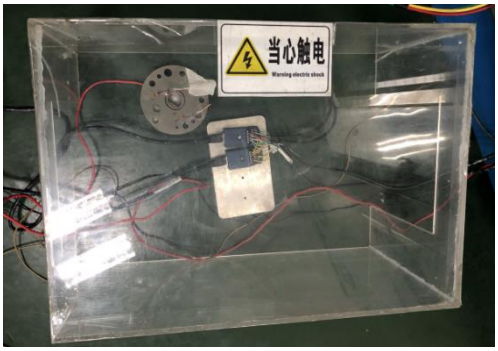

Figure 8 Slip ring calibration bridge circuits

In addition to torque measuring bridge circuit inside the compressor, a slip ring calibration bridge circuit is also required. Attach the same type of strain gauges to a specimen surface with the same material as shaft to form a full bridge circuit, placing it outside the compressor, as shown in Figure 8. Paying attention to the protection of bridge circuit during testing process to prevent measuring deviation caused by human factors. The test flow chart is shown in Figure 9.

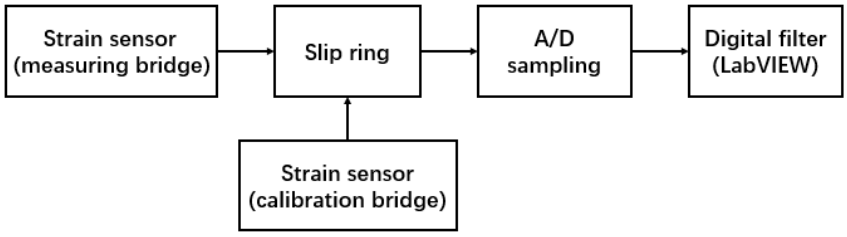

Figure 9 Test flow chart

4.2. Test Signal Acquisition and Analysis System

The virtual instrument (VI) developed by LabVIEW is used to display and process test signal. VI panel is shown in Figure 10, which mainly includes two modules: parameter settings and signal processing. This VI can display test data in real time, and filter high frequency interference signal to obtain an effective waveform. Through internal calculations, the change in torque curve, average torque and shaft power in each second can be observed.

(a) Settings module

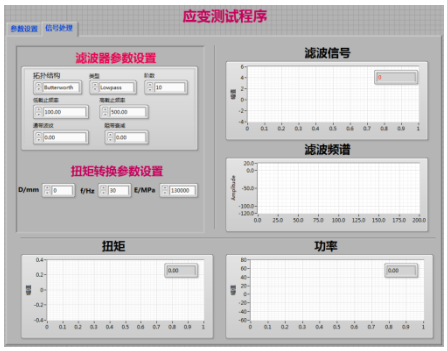

(b) Data processing module

Figure 10 Virtual instrument panel

4.3. Result Analysis

Experimental condition is shown in Table 1.

Table 1 Test condition

Suction pressure	Exhaust pressure	Suction temperature	Exhaust temperature	Frequency	Refrigerant
1.435MPa	2.398MPa	28˚C	51.5˚C	40Hz	R410A

The testing system is zeroed before compressor is turned on. When the compressor performance is stable, the average strain will fluctuate within a stable range, and then data acquisition is processed. There are 50000 data in every 1 second for a total of 25 cycles. The data processing results are shown in Figure 11.

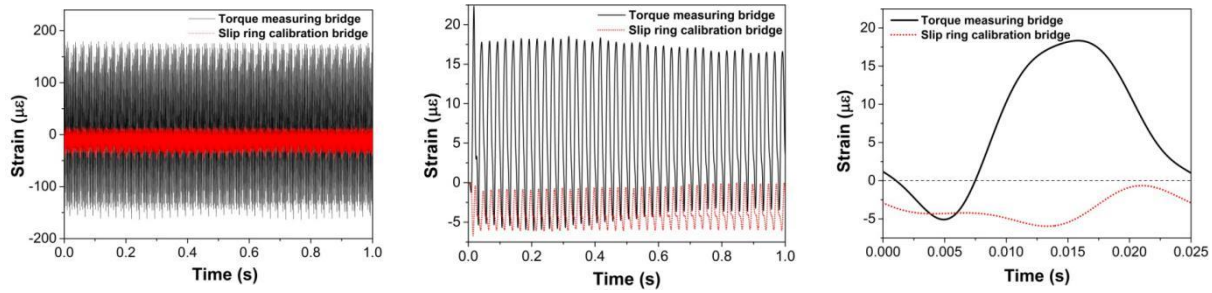

(a) Original curve (b) Filtered curve (c) Curve within a cycle

Figure 11 Test results processing

The torque curve of shaft under a certain operating condition can be directly obtained by the test signal acquisition and analysis system. Figure 11(a) shows the original data. Due to interference of the high-frequency carrier signal, it can be seen that the curve has too much burrs to analyze, so the filtering process is needed. After low-pass filtering, the curve is shown in Figure 11(b). It can be obviously observed the periodic changes of the two curves. Figure 11(c) shows the waveform during one running period, from which it can be seen that calibration of the slip ring has obvious strain fluctuations, so the influence of slip ring cannot be neglected during the torque measuring process.

After the data acquisition, the compressor is turned off. The strain results are quickly reduced and stabilized in a relative short time. Zero drift data of the two bridge circuits are recorded timely, ensuring that the recorded zero drift temperature is consistent with the test temperature. And the results are corrected as follows.

$$\varepsilon_{md} = (\varepsilon_T - \varepsilon_{T0}) - \frac{1}{2}(\varepsilon_S - \varepsilon_{S0}) \tag{11}$$

Wherein： ε_{md} —— corrected strain;

ε_T — torque measuring strain;

ε_{T0}— zero drift of torque measuring bridge circuit;

ε_S— calibration measuring strain of slip ring;

ε_{S0}— zero drift of calibration bridge circuit.

Through correlational calculation with formula(1), the corrected strain is converted into torque. Then torque curve of the shaft in one cycle can be obtained and compared with the theoretical torque curve, as shown in Figure 12.

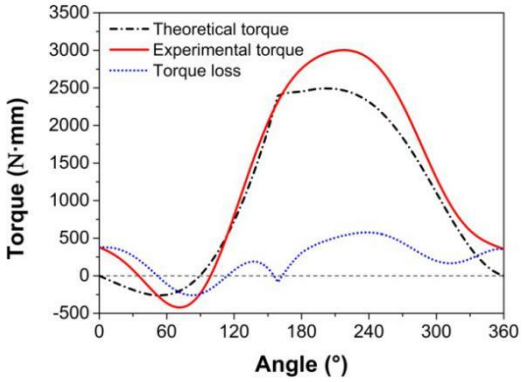

Figure 12 Rotation angle – torque curve

It can be seen from the diagram that the overall trends of test curve and theoretical curve are the same. Due to the additional torque generated by vane, shaft torque increases negatively within 0˚~70˚ in each running period. With pressure in compression chamber increasing, shaft torque increases rapidly. When pump body starts to exhaust, shaft torque decreases rapidly. As the existence of mechanical loss, leakage loss and the suction and exhaust pressure loss, experimental curve is higher than theoretical curve. By subtracting these two curves, torque loss in one cycle can be gotten. As can be seen from Figure 12, the maximum torque loss occurs during the exhaust phase, which may be due to over-compression.

4.4. Power Distribution Analysis

During experiment, compressor's electric power P_{el}=349W is measured by a power meter, which is equal to the sum of motor loss power P_{mo}, mechanical friction loss power P_m and indicated power P_i, namely

$$P_{el} = P_{mo} + P_m + P_i \tag{12}$$

The shaft torque is obtained by experimental test, then shaft power P_e can be calculated. That is the actual output power of motor.

$$P_e = \frac{nT_t}{9549} = P_i + P_m = 320\text{W} \tag{13}$$

Wherein： T_t —— average torque from experimental test.

Compressor indicated power is obtained through the designed P-V experiment, which is a common method in the industry, so it will not be described in detail here. By the P-V experiment, compressor indicated power is P_i=285W, then mechanical friction loss is

$$P_m = P_e - P_i = 35\text{W} \tag{14}$$

Finally, the actual motor efficiency η_e and mechanical efficiency η_m will be obtained.

$$\eta_e = \frac{P_e}{P_{el}} = 91.7\% \quad , \quad \eta_m = \frac{P_i}{P_e} = 89.1\% \tag{15}$$

Combining test data with the above formulas, power distribution of the prototype is as listed in Table 2.

Table 2: Power distribution of compressor

P_{mo}	P_m	P_i	P_e	P_{el}
29W	35W	285W	320W	349W

4.5. System Uncertainty Analysis

The influence of the slip ring is eliminated by using the calibration bridge, but the contact resistance of each channel of the slip ring is considered to be the same in the correction. In fact, it is not guaranteed due to the different contact stress conditions and temperatures during the operation of the compressor, which will bring in inevitable errors.

In the signal processing, although the low-pass filter can remove interference of the high-frequency carrier signal, it also causes a part of the strain signal to be lost, which brings an error.

5. Conclusions

In summary, the stability of slip ring is monitored while measuring shaft torque, which can eliminate the influence of contact resistance change of the slip ring. Then power distribution of the compressor is analyzed with measurement result.

(1) Using contact strain measuring method and virtual instrument developed by LabVIEW platform, a shaft power measuring system of a hermetic compressor is established, which can directly obtain torque curve of the compressor under operating in real time.

(2) During the working process of slip ring, the influence of the contact resistance change cannot be neglected. The stability of slip ring can be monitored in real time by an external static full bridge circuit, and then the measurement result can be corrected, which will be more accurate. The measurement curve is consistent with the overall trend of the theoretical curve.

(3) According to the measurement results, compressor's power distribution is analyzed, and the actual motor efficiency is 91.6%, mechanical efficiency is 89.1%.

Reference

[1] Miu D P and Wu Y Z 2000 Refrigeration Compressor (Beijing: China Machine Press)
[2] Duan G F and Miao Y S 1997 The Review on Torque Measurement Technique Home and Abroad Journal of Test and Measurement Technology 11 44-47
[3] Lv H Y, Yang J and Song N 2017 The Methods and Development Trend of Torque Measurement for Transmission Shafting Metrology & Measurement Technology 37 6-10
[4] Zhu C M, Wang Z X and Hu X F 2009 Design and study of torque measurement system Machinery Design & Manufacture 5 30-32
[5] Meng J and Wang H Q 2012 Signal Collection and Processing for Non-Contact Automotive Torque Sensor Control Engineering of China 19 339-342
[6] Matsushima M, Nomura T, Nishimura N and Iyota H 2000 Direct Torque Measurement of Hermetic Rotary Compressors Using Strain Gauge 15th International Compressor Engineering Conference at Purdue 1427
[7] Zhou X Q and Wang Z Y 2007 Analysis of Main Detection Parameters of Precision Slip Rings, Metrology & Measurement Technology 27 72-73
[8] Stutevant R 2003 Torque Sensor Test Principle and Application, Shanghai Measurement and Testing, 30 42-43
[9] Shan Z H 2009 Material Mechanics (Beijing: Higher Education Press) p 97-100